COMPARATIVE STUDY OF PILOT SYMBOL ASSISTED MODEM SCHEMES

J.M. Torrance, L. Hanzo

University of Southampton, UK

Abstract

The performance of a range of 1, 2 and 4 bit/symbol pilot symbol assisted modulation (PSAM) [1, 3] arrangements employing first-order linear, low pass, polynomial and optimum higher-order linear interpolation schemes is analysed in contrast to that of the equivalent non-coherent modems. Both the non-coherent modems as well as the coherent PSAM schemes exhibited a residual bit error rate (BER), but the best compromise in terms of performance, system delay and complexity was attributable to the first-order linear interpolator. In case of short interpolation buffers the polynomial interpolator slightly outperformed the low-pass and the higher-order linear optimum interpolators, but this advantage erodd in case of longer buffers. The higher complexity of the minimum mean squared error interpolator is not justifiable in terms of performance improvements. The low-complexity linearly interpolated PSAM schemes have an improved performance in comparison to the differential schemes in case of higher order constellations, such as 4- and 16-level quadrature amplitude modulation (QAM).

1 Motivation

The potential of re-configurable multilevel linear modulation schemes in adaptive multi-mode transceivers has been the subject of various studies [1]. This treatise endeavours to compare the performance of 1, 2 and 4 bit/symbol coherent pilot symbol assisted modulation (PSAM) [1, 3] arrangements employing first-order linear, low pass, polynomial and optimum higher-order linear interpolation schemes to that of the equivalent lower complexity non-coherent modems.

The paper is organised as follows. Section 2 provides a brief system overview, Section 3 describes the minimum mean squared error channel gain estimation and Section 4 summarises the system parameters used. Detailed performance figures are provided in Section 5, before concluding in Section 6.

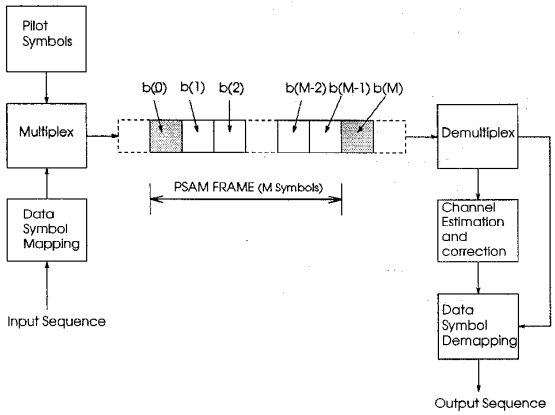

Figure 1: Schematic of a PSAM System showing the PSAM Frame

2 PSAM System Description

The block diagram of a general PSAM scheme is depicted in Figure 1, where the pilot symbols P are cyclically inserted into the data sequence prior to pulse shaping. A frame of data is constituted by M symbols, and the first one in every frame is assumed to be the pilot symbol $b(0)$, followed by $(M-1)$ useful data symbols $b(1), b(2) \ldots b(M-1)$.

Detection can be carried out by matched filtering, and the output of the matched filter is split in data and pilot paths, as seen in Figure 1. The set of pilot symbols can be extracted by decimating the matched filter's sampled output sequence using a decimation factor of M. The extracted sequence of pilot symbols must then be interpolated in order to derive a channel estimate $v(k)$ for every useful received information symbol $r(k)$. This contribution endeavours to compare the performance of the simple linear, low-pass, polynomial and the highest complexity optimum linear interpolator [3]. Finally, decision is carried out against a decision level reference grid, scaled and rotated according to the instantaneous channel estimate $v(k)$.

The received data symbols must be delayed according to the interpolation and prediction delay incurred. This delay becomes longer, if interpolation is carried out using a longer history of the received signal to yield better channel estimates. Consequently,

there is a trade-off between processing delay and accuracy. The interpolation coefficients can be kept constant over a whole pilot-period of length M, but better channel estimates can be obtained if the interpolator's coefficients are optimally updated for every received symbol.

The complex envelope of the modulated signal can be formulated as:

$$m(t) = \sum_{k=-\infty}^{\infty} b(k)p(t-kT), \tag{1}$$

where $b(k)$ represents the I or Q components of the symbols to be transmitted, T is the symbol duration and $p(t)$ is a band-limited unit-energy signalling pulse, for which we have:

$$\int_{-\infty}^{\infty} |p(t)|^2 dt = 1. \tag{2}$$

For a narrowband Rayleigh channel the received signal is given by:

$$r(t) = c(t) \cdot m(t) + n(t), \tag{3}$$

where $n(t)$ is the AWGN and $c(t)$ is the channel's complex gain. Assuming a Rayleigh-fading envelope $\alpha(t)$ and uniformly distributed phase $\phi(t)$ we have:

$$c(t) = \alpha(t)e^{j\phi(t)}. \tag{4}$$

The matched filter's output symbols at the sampling instant kT are then given as:

$$r(k) = b(k) \cdot c(k) + n(k). \tag{5}$$

It is convenient to assume [3] that in every channel sounding block $b(0)$ is the pilot symbol and consider the detection of the useful information symbols in the range $\lfloor -M/2 \rfloor \leq k \leq \lfloor (M-1)/2 \rfloor$, where $\lfloor \bullet \rfloor$ is the integer part of $\bullet$.

3 Channel Gain Estimation

Optimum detection is achieved if the corresponding channel gain $c(k)$ is estimated for every received symbol $r(k)$ in the above range. Assuming a linear model, the channel gain estimate $v(k)$ can be derived as a weighted sum of the surrounding K received pilot symbols $r(iM)$, $\lfloor -K/2 \rfloor \leq i \leq \lfloor K/2 \rfloor$, as shown below:

$$v(k) = \sum_{i=\lfloor -K/2 \rfloor}^{\lfloor K/2 \rfloor} h(i,k) \cdot r(iM), \tag{6}$$

and the weighting coefficients $h(i,k)$ explicitly depend on the symbol position k within the frame of M symbols.

The estimation error $e(k)$ associated with the gain estimate $v(k)$ is computed as:

$$e(k) = c(k) - v(k). \tag{7}$$

While previously proposed PSAM schemes used either a low-pass interpolation filter [4] or an approximately Gaussian filter [5], Cavers employed an optimum Wiener filter to minimise the channel estimation error variance $\sigma^2{}_e(k) = E\{e^2(k)\}$, where $E\{\ \}$ represents the expectation. This well-known estimation error variance minimisation problem can be formulated as follows:

$$\begin{aligned} \sigma_e^2(k) &= E\{e^2(k)\} = E\{[c(k) - v(k)]^2\} \\ &= E\left\{ \left[c(k) - \textstyle\sum_{i=\lfloor -K/2 \rfloor}^{\lfloor K/2 \rfloor} h(i,k) \cdot r(iM) \right]^2 \right\}. \end{aligned} \tag{8}$$

In order to find the optimum interpolator coefficients $h(i,k)$, minimising the estimation error variance $\sigma^2{}_e(k)$ we consider estimating the k^{th} sample and set:

$$\frac{\partial \sigma_e^2(k)}{\partial h(i,k)} = 0 \quad \text{for} \quad \lfloor -K/2 \rfloor \leq i \leq \lfloor K/2 \rfloor. \tag{9}$$

Then using Equation 8 we have:

$$\begin{aligned} &\frac{\partial \sigma^2{}_e(k)}{\partial h(i,k)} = 0 \\ &= E\left\{ 2 \left[c(k) - \sum_{i=\lfloor -K/2 \rfloor}^{\lfloor K/2 \rfloor} h(i,k) \cdot r(iM) \right] \cdot r(jM) \right\}. \end{aligned}$$

After multiplying both square bracketed terms with $r(jM)$, and computing the expected value of both terms separately, we arrive at

$$E\{c(k) \cdot r(jM)\} = E\{ \sum_{i=\lfloor -K/2 \rfloor}^{\lfloor K/2 \rfloor} h(i,k) \cdot r(iM) \cdot r(jM) \}. \tag{10}$$

Observe that

$$\Phi(j) = E\{c(k) \cdot r(jM)\} \tag{11}$$

is the cross-correlation of the received pilot symbols and complex channel gain values, while

$$R(i,j) = E\{r(iM) \cdot r(jM)\} \tag{12}$$

represents the pilot symbol autocorrelations, hence Equation 10 yields:

$$\sum_{i=\lfloor -K/2 \rfloor}^{\lfloor K/2 \rfloor} h(i,k) \cdot R(i,j) = \Phi(j), \quad j = \lfloor -\frac{K}{2} \rfloor \cdots \lfloor \frac{K}{2} \rfloor. \tag{13}$$

If the fading statistics can be considered stationary, the pilot autocorrelations $R(i,j)$ will only depend on the difference $|i-j|$, giving $R(i,j) = R(|i-j|)$. Therefore Equation 13 can be written as:

$$\sum_{i=\lfloor -K/2 \rfloor}^{\lfloor K/2 \rfloor} h(i,k) \cdot R(|i-j|) = \Phi(j), \quad j = \lfloor -\frac{K}{2} \rfloor \cdots \lfloor \frac{K}{2} \rfloor, \tag{14}$$

which is a form of the well-known Wiener-Hopf equations, often used in estimation and prediction theory.

This set of K equations contains K unknown prediction coefficients $h(i,k)$, $i = \lfloor -K/2 \rfloor \ldots \lfloor K/2 \rfloor$, which must be determined in order to arrive at a minimum error variance estimate of $c(k)$ by $v(k)$.

First the correlation terms $\Phi(j)$ and $R(|i-j|)$ must be computed and hence the expectation value computations in Equations 11 and 12 need to be restricted to a finite duration window. The pilot autocorrelation, $R(i,j)$, may then be calculated from the fading estimates at the pilot positions within this window. Calculation of the received pilots' and the complex channel gains' cross correlation is less straight forward, because in order to calculate the cross-correlation the complex channel gains have to be known at the position of the data symbols as well as the pilot symbols. However, the channel gains are only known at the pilot positions, while for the data symbol positions they must be derived by interpolation. Hence we fitted a polynomial to the known samples of $R(|i-j|)$ and then estimated the values of $\Phi(j)$ for the unknown positions.

The set of Equations 14 can also be expressed in a convenient matrix form as:

$$\begin{bmatrix} R(0) & R(1) & R(2) & \ldots & R(K) \\ R(1) & R(0) & R(1) & \ldots & R(K-1) \\ R(2) & R(1) & R(0) & \ldots & R(K-2) \\ \vdots & \vdots & \vdots & \ldots & \vdots \\ R(K) & R(K-1) & R(K-2) & \ldots & R(0) \end{bmatrix} \cdot \begin{bmatrix} h\left(\lfloor -\frac{K}{2} \rfloor, k\right) \\ h\left(\lfloor -\frac{K}{2}+1 \rfloor, k\right) \\ h\left(\lfloor -\frac{K}{2}+2 \rfloor, k\right) \\ \vdots \\ h\left(\lfloor \frac{K}{2} \rfloor, k\right) \end{bmatrix} = \begin{bmatrix} \Phi\left(\lfloor -\frac{K}{2} \rfloor\right) \\ \Phi\left(\lfloor -\frac{K}{2}+1 \rfloor\right) \\ \Phi\left(\lfloor -\frac{K}{2}+2 \rfloor\right) \\ \vdots \\ \Phi\left(\lfloor \frac{K}{2} \rfloor\right) \end{bmatrix},$$

which can be solved for the optimum predictor coefficients $h(i,k)$ by matrix inversion using Gauss-Jordan elimination or any appropriate recursive algorithm. Once the optimum predictor coefficients $h(i,k)$ are known, the minimum error variance channel estimate $v(k)$ can be derived from the received pilot symbols using Equation 6, as also demonstrated by Figure 1.

4 System Parameters

We restricted our investigations to a set of worst-case channel conditions characteristic of the Pan-American IS-54 system, where the signalling rate was set to 20 kBd. The propagation frequency was increased from 900 MHz to 1.8 GHz and the vehicular speed was fixed at 50 km/h. The corresponding Doppler frequency is 83.3 Hz, giving a relative Doppler frequency of 0.0042. In comparison, the GSM-like DCS1800 system under identical propagation conditions results in a relative Doppler frequency of 0.0003, which is associated with a less dramatically fading signal envelope and hence better fade tracking properties. The corresponding Doppler filter emulated a vertical loop antenna in a plane perpendicular to the vehicle's motion and, apart from the channel's phase rotations, perfect carrier and clock recovery were assumed.

In case of the **linear interpolator** the system delay was minimised, since only one PSAM frame had to be buffered in order to be able to derive a channel estimate for each information symbol between the pilots. For the **low pass interpolation** we had to resolve, what impulse response window function and length constituted the best compromise in delay and performance terms. When using a Buffer length of 5 PSAM frames as well as a pilot separation or Gap of 40 symbols and evaluating the mean absolute error, the mean squared error and the maximum error between the real fading file and the interpolated file, the Hamming window was found superior to the Hanning window. Hence in our further endeavours we opted for the Hamming window.

Four interpolation methods, namely linear, low pass, polynomial and Cavers' minimum mean squared error (mmse) linear interpolation were simulated and compared in the context of pilot assisted binary phase shift keying (BPSK), 4-level quaternary phase shift keying (QPSK) and 16-level quadrature amplitude modulation (16QAM). The 1 bit/symb, 2 bit/symb and 4 bit/symb modulation schemes were combined with all four interpolators and their bit error rate (BER) performance was evaluated at channel signal to noise ratios (SNR) of 20, 30 and 40 dB, which yielded $3 \cdot 4 \cdot 3 = 36$ sets of results. In each set of results pilot Buffer lengths of 3, 5, 7, 9, 11 PSAM frames and pilot separation or Gap values of 10, 20, 40, 60, 80, 100, 116 were employed, leading to a plethora of performance curves, which allowed us to generate a corresponding set of 3-dimensional (3D) graphs of BER versus Buffer and Gap.

Furthermore, in order to establish the relative merits of PSAM compared to non-coherent modulation, the performance of differential BPSK (DBPSK), differential QPSK (DQPSK) and differential 16 Star QAM [1] were also evaluated and the corresponding BER figures will be compared in the next Section.

5 Results and Discussion

Our results are shown for 16QAM in Figure 2, and similar tendencies were observed for QPSK and BPSK as well. Results for the latter two schemes will be presented only in a more compact form for reasons of space economy. As expected, for all modulation schemes and interpolation techniques, as well as at all Buffer and Gap values, the BER reduces with increasing channel SNR. Furthermore, increasing the Buffer length and reducing the pilot Gap will typically reduce the BER, but all scenarios exhibited a BER floor. Furthermore, the residual BER (RBER)

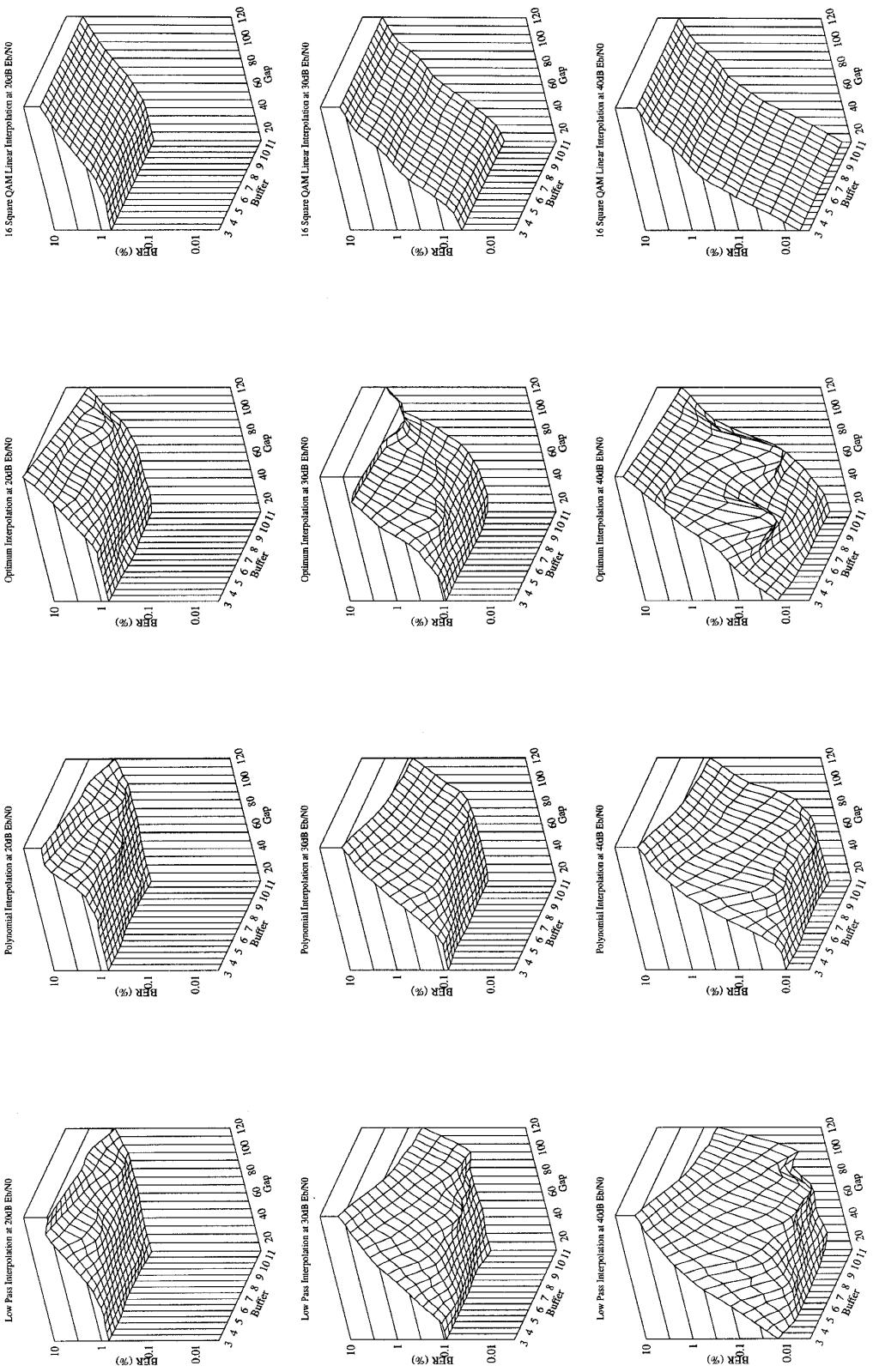

Figure 2: BER versus Buffer length and pilot Gap performance of pilot-assisted 16QAM over Rayleigh channels at 20 kBd, 50 km/h, 1.8 GHz

Interpolation technique	$\frac{E_b}{N_0}$[dB]		
	20	30	40
Linear RBER [%]	0.41	0.042	0.0040
Polynomial RBER [%]	0.43	0.040	0.0045
Low pass RBER [%]	0.43	0.040	0.0045
Optimum RBER [%]	0.43	0.040	0.0045

Table 1: RBER of pilot-assisted BPSK over narrowband Rayleigh fading channel using Linear, Polynomial, Low pass and Optimum Linear Interpolation at 20 kBd, 50 km/h, 1.8 GHz

Interpolation technique	$\frac{E_b}{N_0}$[dB]		
	20	30	40
Linear RBER [%]	0.32	0.039	0.0049
Polynomial RBER [%]	0.35	0.040	0.0050
Low pass RBER [%]	0.35	0.040	0.0050
Optimum RBER [%]	0.35	0.040	0.0050

Table 2: RBER of pilot-assisted QPSK over narrowband Rayleigh fading channel using Linear, Polynomial, Low pass and Optimum Linear Interpolation at 20 kBd, 50 km/h, 1.8 GHz

did not depend on the interpolation scheme used.

In order to present our findings in as terse a form as possible, for each of the modulation schemes and interpolation techniques the RBER was inferred and summarised in Tables 1-3. Note, however that the Buffer and Gap values required to achieve the RBER are dependent upon the type of interpolation technique used. Hence the system delay and complexity explicitly depend on the choice of the interpolation scheme.

The RBER values inferred from Figure 2 and from the corresponding, but not displayed 3D-graphs for QPSK and BPSK, can be portrayed more conveniently in terms of bit energy per noise spectral density (E_b/N_0), as shown in Figure 3. As expected,

Interpolation technique	$\frac{E_b}{N_0}$[dB]		
	20	30	40
Linear RBER [%]	0.62	0.041	0.006
Polynomial RBER [%]	0.68	0.090	0.009
Low pass RBER [%]	0.68	0.080	0.009
Optimum RBER [%]	0.68	0.080	0.009

Table 3: RBER of pilot-assisted 16QAM over narrowband Rayleigh fading channel using Linear, Polynomial,Low pass and Optimum Linear Interpolation at 20 kBd, 50 km/h, 1.8 GHz

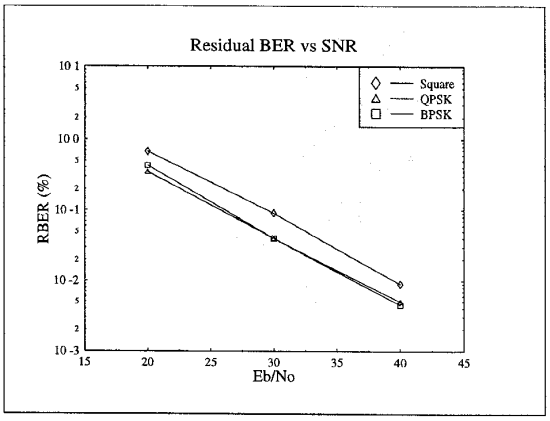

Figure 3: RBER for 1, 2 and 4 Bits Per Symbol Modulation Schemes versus Eb/No.

BPSK and the QPSK are very similar, since QPSK is constituted by two orthogonal BPSK systems. Observe that 16QAM requires an about 3.5 dB higher E_b/N_0 value and a further 6 dB higher channel SNR value.

We observed that in case of small Buffer sizes the polynomial interpolator succeeded for all modulation schemes and at all SNRs to reduce the BER to the value of the RBER, while maintaining the largest gap. This is because in case of short buffers, ie when the channel estimates are only available for a limited number of pilot symbols, the non-linear polynomial model will out perform the linear model or a severely truncated short impulse response. As the Buffer size is increased, the high-order coefficients of the polynomial interpolator diminish and hence increasing the Buffer size becomes less significant. On the same note, as the Buffer size increases, the impulse response of the low pass interpolator becomes more like that of an ideal Sinc function and therefore its performance improves.

As the modulation constellation becomes less complex, ie the number of bits per symbol is reduced, the benefits of coherent modulation are reduced, as evidenced by Table 4, and Figure 4, although this is also a function of the channel SNR. Surprisingly, for BPSK at an SNR of 20 dB, the differential scheme has actually a marginally better BER performance than the corresponding PSAM scheme, even when disregarding the proportion of power allocated to the pilots. In contrast, for higher order constellations, such as QPSK and 16QAM, PSAM does reduce the RBER and has a better performance than star 16QAM, while having a somewhat higher delay and similar complexity, when using linear interpolation.

$\frac{E_b}{N_0}$[dB]	Differential		
	BPSK RBER[%]	QPSK RBER[%]	16 Star RBER[%]
20	0.38	0.42	1.2
30	0.05	0.058	0.18
40	0.011	0.012	0.03
$\frac{E_b}{N_0}$[dB]	PSAM		
	BPSK RBER[%]	QPSK RBER[%]	16 Square RBER[%]
20	0.43	0.35	0.68
30	0.04	0.04	0.09
40	0.0045	0.005	0.009

Table 4: RBER for PSAM Schemes and Differential Schemes, of various modulation constellations and at various SNRs over a Narrowband Rayleigh fading channel at 20 kBd, 50 km/h, 1.8 GHz

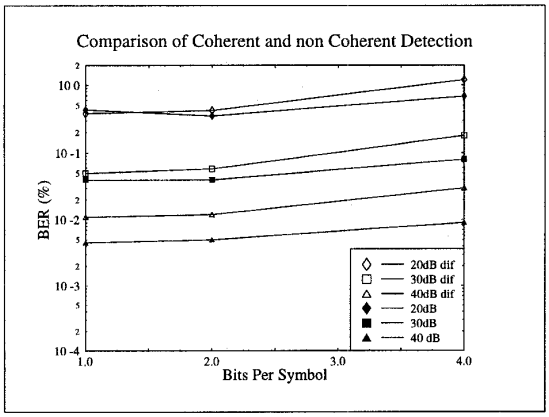

Figure 4: RBER for 1,2 and 4 Bits Per Symbol PSAM Modulation Compared With Equivalent Differential Schemes

6 Summary and Conclusions

In conclusion, both the non-coherent differential modems and the coherent pilot-assisted BPSK, QPSK and 16QAM modems exhibited a residual bit error rate. The shortest system delay and lowest complexity amongst the PSAM schemes was associated with the one employing the first-order linear interpolator. For higher-order phasor constellations, such as that of QPSK and 16QAM the linearly interpolated PSAM arrangement outperformed the corresponding non-coherent scheme, while exhibiting a similar complexity. Future work is targeted at a similar study of block-coded modulation schemes.

7 Acknowledgement

The financial support of the EPSRC, UK in the framework of the research contract GR/J46845 is gratefully acknowledged.

References

[1] **W.T. Webb, L. Hanzo**: "Modern Quadrature Amplitude Modulation - Principles and applications for fixed and wireless communications", *IEEE Press-Pentech Press*, 1994

[2] **W.T. Webb, L. Hanzo, R. Steele**: "Bandwidth-Efficient QAM Schemes for Rayleigh-Fading Channels", *IEE Proc. Pt I*, Vol 138, No 3, June, 1991, pp 169-175

[3] **J.K. Cavers**: "An Analysis of Pilot Symbol Assisted Modulation for Rayleigh Fading Channels", *IEEE Tr. on Veh. Techn.*, Vol. 40, No. 4, pp. 686-693, Nov. 1991

[4] **M.L. Moher, J.H. Lodge**: "TCMP – A Modulation and Coding Strategy for Rician Fading Channels", *IEEE J. Select. Areas Commun.*, Vol.7, pp. 1347-1355, Dec. 1989

[5] **S. Sampei, T. Sunaga**: "Rayleigh Fading Compensation Method for 16-QAM in Digital Land Mobile Radio Channels", *Proc. IEEE Veh. Technol. Conf.*, San Francisco, CA, May 1989, pp. 640-646